Volume 58
Number 9
28 January 2022
Pages 1229–1428

ChemComm

Chemical Communications

rsc.li/chemcomm

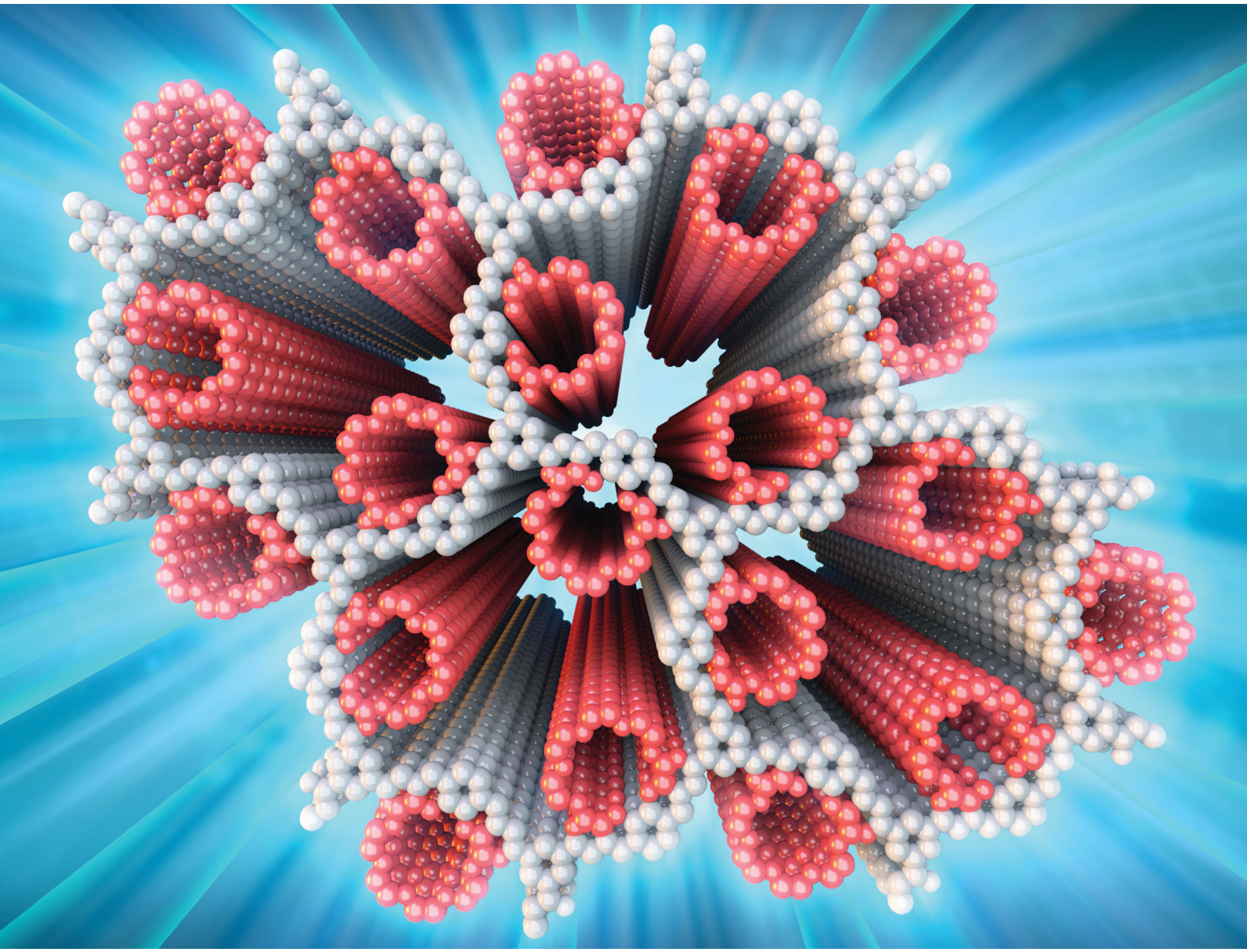

ISSN 1359-7345

ROYAL SOCIETY OF CHEMISTRY

COMMUNICATION

Chunyan Chi *et al.*

Enhanced emission by stacking of crown ether side chains in a 2D covalent organic framework

ChemComm

COMMUNICATION

View Article Online
View Journal | View Issue

Cite this: *Chem. Commun.*, 2022, **58**, 1302

Received 26th June 2021,
Accepted 20th December 2021

DOI: 10.1039/d1cc03409j

rsc.li/chemcomm

Enhanced emission by stacking of crown ether side chains in a 2D covalent organic framework†‡

Liu Yuan,§[ab] Jun Zhu,§[a] Shaofei Wu[a] and Chunyan Chi *[a]

Hydrazone compounds could be highly emissive in the solid state. However, most hydrazone-linking COFs are poorly luminescent. Here we report the enhancement of fluorescence in a 2D hydrazone-linking COF by side chain engineering. Stacking of the bulky and semi-rigid crown ether side chains restricts intramolecular rotation of the backbone around the hydrazone linkers, reducing the thermal dissipation and achieving 20-fold improved emission.

Photoluminescence (PL) covalent organic frameworks (COFs) are emerging porous crystalline materials showing specific sensing and detection abilities towards heavy metals,[1–3] toxic gases,[4] explosives,[5,6] radicals,[7] humidity,[8] pH,[9] bio-substances,[10] *etc.* Besides general applications found for porous materials,[11–14] the light emitting property also endows them with potential applications in imaging, lasing and optoelectronics.[15] The straightforward way to design highly photoluminescent COF materials is to incorporate strong emissive monomers. Despite occasional successes, this strategy fails in many cases mainly for two reasons. One is due to aggregation caused quenching induced by π–π stacking of monomers. The other one is available thermal dissipation pathways due to rotational labile linking. In the course of developing strong emissive COFs, methods like applying aggregation-induced emission (AIE) monomers,[4] 3D topology,[16] avoiding eclipsed stacking,[17] rigidifying linkers,[18] "pinpoint surgery"[19] and rotational restriction by hydrogen bonding[20] have been used or discovered. These methods lead to synthesis of highly emissive, even white emissive COFs. Despite this profound progress, new strategies for improving the PL intensity of COF materials are still valuable.

Hydrazone-linking COFs, first reported by Uribe-Romo *et al.*, could be highly crystalline and display excellent chemical and thermal stability.[21] Due to these advantages, they are widely studied as a platform for a variety of applications.[22–31] Hydrazone compounds are rotational-free and generally non-emissive in solution, but could be highly emissive in the solid state. This phenomenon is shown in Fig. S1 (ESI‡) for model compound **MC2OMe**. The emission in the aggregation state is due to restriction of intramolecular rotation (RIR) around single bonds. However, as a crystalline aggregation of hydrazone compounds by covalent linkages, most hydrazone COFs are weakly or non-emissive due to inefficient restriction of the bond rotation around hydrazone linkers. Besides, photo-induced electron transfer between the hydrazone linker and backbone moieties could also cause emission weakening.[19] Li *et al.* developed highly emissive hydrazone COFs (PLQY up to 16.3%) by restriction of intramolecular bond rotation *via* intralayer and interlayer hydrogen bonds among highly organized layers.[20] Jiang's group discovered that the emission of a hydrazone COF could be turned on by N–H bond deprotonation which eliminated the photo-induced electron transfer pathway.[19]

Here, we aim to enhance the PL intensity of hydrazone-linked COFs by side chain engineering. Four hydrazone COFs with the same skeleton but different side chains (**R**), as well as their model compounds, were synthesized (Scheme 1 and ESI‡). **COF2OMe** can represent the structural expansion and stacking of model compound **MC2OMe**. But unlike **MC2OMe** crystalline powder, this COF material is nearly non-emissive. When the two methoxyl groups were changed to bigger semi-rigid[32] crown ether chains, the absolute PL quantum yield (QY) of the COFs improved, with larger crown ether chains leading to higher PLQY. A decent PLQY of 10.1% was found for **COF21C7**, close to its model compound **MC21C7** (11.4%) in the crystalline state.

All four COF materials have been successfully synthesized by imine condensation between benzene-1,3,5-tricarbohydrazide

[a] *Department of Chemistry, National University of Singapore, 3 Science Drive 3, 117543, Singapore, Singapore. E-mail: chmcc@nus.edu.sg*
[b] *State Key Laboratory of Electronic Thin Films and Integrated Devices, School of Optoelectronic Science and Engineering, University of Electronic Science and Technology of China, Chengdu 610054, China*

† Dedicated to Prof. Seth Marder on the occasion of his 60th birthday.

‡ Electronic supplementary information (ESI) available: Synthetic procedures and structural characterization data; additional physical characterization data; calculation details. See DOI: 10.1039/d1cc03409j [ξ] Dedicated to Prof. Seth Marder on the occasion of his 60th birthday.

§ These authors contributed equally to this work.

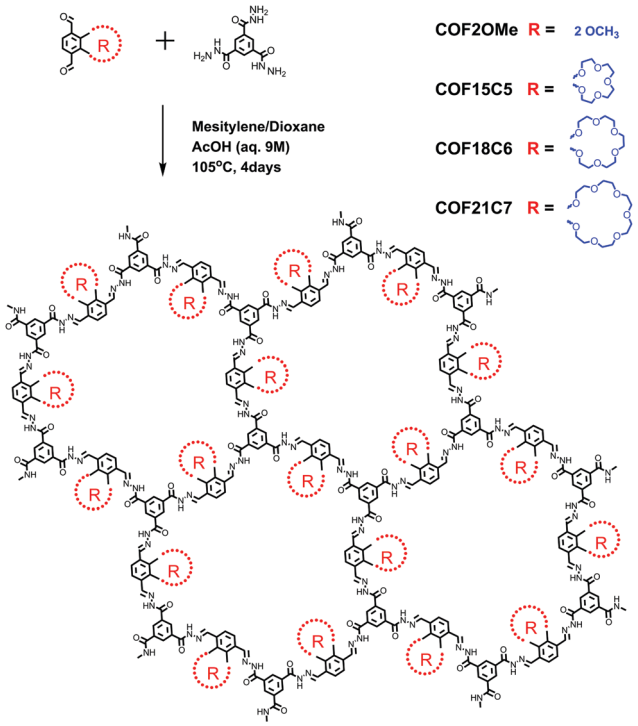

Scheme 1 Synthesis and structure of model compounds and COF materials.

and the corresponding di-aldehyde under solvothermal conditions (see the ESI‡). Fourier transform infrared (FT-IR) spectra of the COFs, monomers and model compounds were obtained to confirm the formation of the COFs (Fig. S2–S5, ESI‡). For all of the COFs, their FT-IR spectra showed broad stretching vibration band of the imine bond (–C═N–) at 1650–1685 cm^{-1}, which merged with the carbonyl (C═O) stretch at 1652 cm^{-1} to form broad bands. Similar situation was also found for FT-IR spectra of other hydrazone COFs.[22,27,28] This was further confirmed by their good agreement with the FT-IR spectra of the corresponding model compounds, which did not show the more commonly found (C═N) stretch at ~1610–1625 cm^{-1} either. Furthermore, the disappearance of the strong (N–H) stretching peak at 3300 cm^{-1} and aldehyde (CH═O) stretching at ~1700 cm^{-1}, and the retention of (CON–H) stretching at 3205–3210 clearly demonstrates the consuming of monomers and the formation of the *–CO–*NH–N═C– linking structure in the COFs. Bands at 2879–2950 cm^{-1} were assigned to the (OC–H) stretch of the side chains. And their relative intensity compared to low frequency bands increased as the COF's side chains grow bigger, in agreement with more $–CH_2–$ groups for larger crown ethers. To further confirm the chemical structure of these COFs, cross polarization magic angle spinning (CP-MAS) ^{13}C NMR spectra of the solid samples were measured (Fig. S6, ESI‡). The peak at ~157 ppm corresponding to C═N linkages was observed for all COFs. Clear peaks were observed for **COF2OMe**, where the two signals at 164 ppm and 149 ppm were assigned to C═O and side chain **R**-substituted benzene carbons, respectively, and the four peaks between 105 and 131 ppm were for the other aromatic carbons. For the crown ether COFs, peaks of C═O carbon broadened and all peaks of crown ether dwelling benzene carbons shifted to lower fields. This might be caused by multiple conformations presented in the crown ether chains and backbone conformation "freezing" by tight stacking of these large semi-rigid cyclic groups. Elemental analysis reveals that the contents of carbon, hydrogen, and nitrogen of the COFs are close to the theoretically calculated values (ESI‡).

Powder X-ray diffraction (PXRD) analyses were performed to determine the crystallinity of the COFs (Fig. 1). The experimental

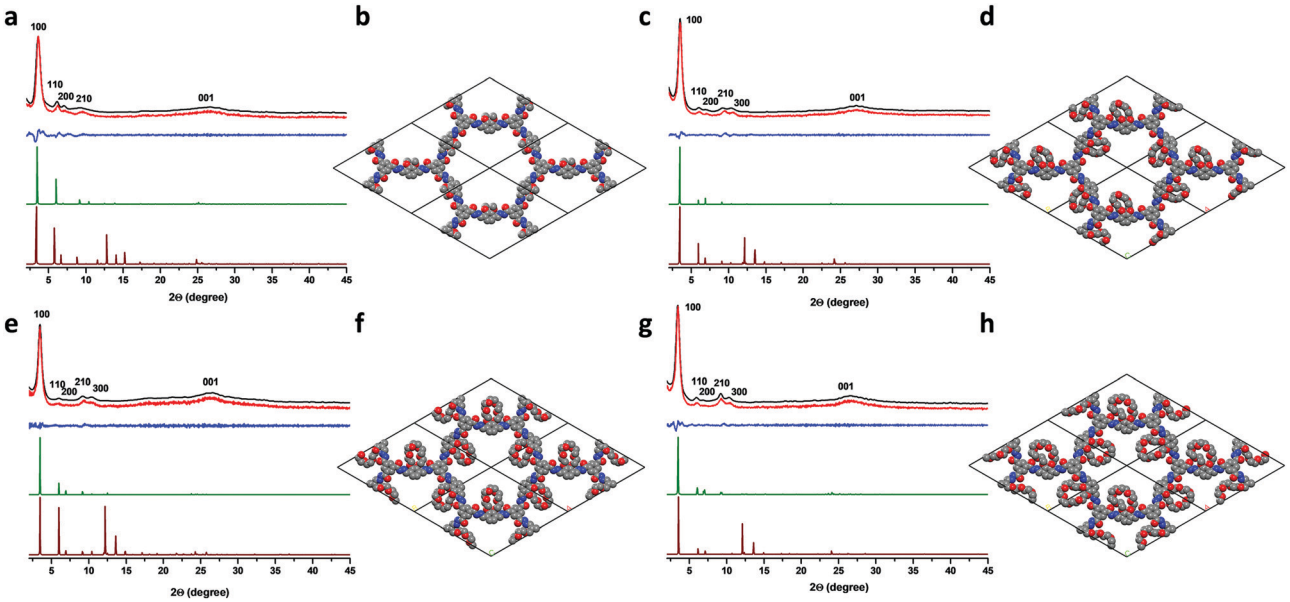

Fig. 1 Powder XRD patterns of experimental (black), Pawley-refined (red), their difference (blue), simulated eclipsed (green) and staggered (brown) stacking for (a) **COF2OMe**, (c) **COF15C5**, (e) **COF18C6** and (g) **COF21C7**. Simulated crystal structures of (b) **COF2OMe**, (d) **COF15C5**, (f) **COF18C6** and (h) **COF21C7**.

PXRD pattern of **COF2OMe** showed peaks at 3.60°, 6.15°, 7.14°, 9.34° and 26.3°, which could be assigned to the (100), (110), (200), (210) and (001) planes, respectively (Fig. 1a). The corresponding interlayer distance is 3.5 Å, calculated from the (001) diffraction. Very similar PXRD patterns were found for the other three COFs (Fig. 1c, e and g), but one more peak at around 10.5° was found in these materials, which was assigned to the (300) diffraction. All the (001) peaks were broad and located at very close positions, indicating similar interlayer packing distances around 3.5 Å. The sharp (100) diffraction peaks did show a decrease of angles from 3.60 to 3.53, 3.48 and 3.46 for **COF2OMe**, **COF15C5**, **COF18C6** and **COF21C7**, respectively. Thus, the increase of the side chain size might have caused slight expansion of the backbone frames. To determine the crystal structure of the COFs, theoretical simulations were carried out to compare with the experimental ones. For all the COFs, the simulated PXRD patterns of the eclipsed structures (AA stacking) were in good agreement with the experimental PXRD patterns, either in peak positions or in relative intensities, while simulated staggered packing (AB stacking) showed deviations in relative intensities (Fig. 1a, c, e and g). Moreover, the Pawley refined PXRD profiles for AA stacking matched the experimental ones very well as evidenced by their negligible difference, with R_{wp} of 7.92%, 4.04%, 7.34%, 5.46% and R_p of 5.29%, 3.08%, 5.54%, 4.32% for **COF2OMe**, **COF15C5**, **COF18C6** and **COF21C7**, respectively. It is worth noting that the AA stacking structure is generally found in hydrazone COFs. This eclipsed packing mode lays the foundation for restriction of backbone rotation by close staking.

Though multiple diffraction peaks were observed for these COFs, their crystallinity was only at a moderate-to-low level. Full loading of finely-ground COF powders only gave a diffraction intensity of less than 4000 counts for all the (100) peaks, measured on a Bruker D8 Focus Powder X-ray diffractometer at 0.15° min^{-1} using Cu Kα radiation (40 kV, 40 mA). Besides, the crystallinity was also reflected by the low BET surface area for the COFs. Nitrogen adsorption–desorption measurements were carried out to investigate the porosity of these COF materials at 77 K, after activation by degassing the COF sample at 120 °C for 8 h. The sorption isotherms (Fig. S7, ESI‡) were all classified as type I nitrogen sorption isotherms according to the IUPAC classification. Though quite weak, a steep uptake of nitrogen gas at low pressure was observed for all COFs, indicating that the materials were microporous. Utilizing the Brunauer–Emmett–Teller (BET) model, low specific surface areas of 82, 18, 21 and 14 m^2 g^{-1} were calculated for **COF2OMe**, **COF15C5**, **COF18C6** and **COF21C7**, respectively. A nonlocal density functional theory (NLDFT) model was fitted to the isotherms of the COFs to estimate their pore size distributions. Only **COF2OMe** displayed a distinguishable pore size distribution profile centered at 2.63 nm, in good agreement with the expected pore sizes observed in the crystal simulations (Fig. S8, ESI‡). No centered pore size distributions were determined by NLDFT for the crown ether COFs. Despite oligomers that might reside inside the pores due to hydrogen-bonding interactions,[26,33] bulk crown ethers occupied a large space in the pores, resulting in low BET surface area.

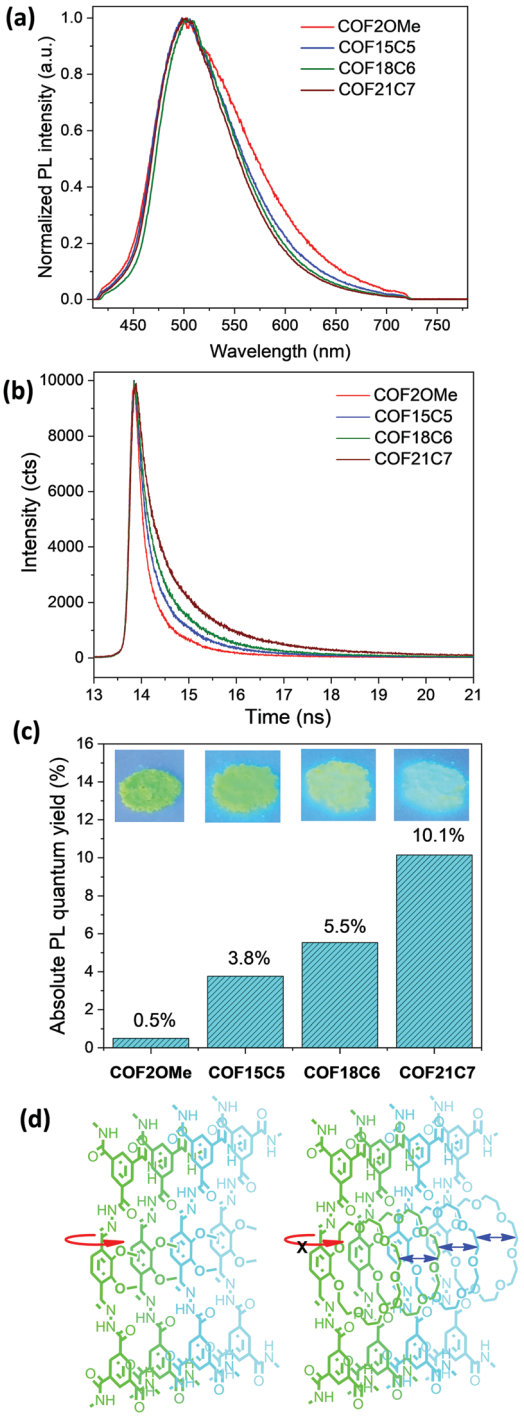

Fig. 2 (a) Solid state photoluminescence spectra, (b) fluorescence decay curves, (c) absolute fluorescence quantum yield with inset fluorescence images of **COF2OMe**, **COF15C5**, **COF18C6** and **COF21C7** powders. (d) Schematic presentation of backbone rotation restriction by stacking of semi-rigid crown ether chains (red arrow indicates possible rotation mode, blue arrows represent repulsion force).

The morphology of the COFs was revealed by scanning electron microscopy (SEM) (Fig. S9, ESI‡). Nanoparticles and rods with non-uniform morphologies were observed for the **COF2OMe**. Nanoparticle (50–200 nm) aggregates were generally found for the other three COFs. The lack of regular and uniform

shapes for these nanoparticles also indicates that these materials are not highly crystalline.

The luminescence property of these COF materials was investigated by solid-state fluorescence spectroscopy. When excited by 365 nm ultraviolet lamps, cyan to green luminescence with very similar PL bands centred at 503 nm was observed for all the COF powders (Fig. 2a). The luminescence brightness increased drastically as shown in the images (Fig. 2c inset). Thus, we measured the absolute PLQY of them in the solid state and the results were shown in Fig. 2c. **COF2OMe** exhibited a very low PLQY of 0.5%, which was slightly higher than the value of 0.4% for a hydrazone COF with very similar structure.[20] Compared with **COF2OMe**, the latter three COFs exhibited successive increase of PLQY from 3.8% for **COF15C5**, to 5.5% for **COF18C6**, and finally to 10.1% for **COF21C7**, with a 20.2-fold improvement of PLQY from **COF2OMe** to **COF21C7**. In addition, a trend of band narrowing of the PL spectra from **COF2OMe** to the other three COFs was also observed (Fig. 2a), possibly due to more rotational freedom that leads to more energy relaxation pathways of the former, as depicted in Fig. 2d. The three crown ether COFs were tested for metal ion sensing, but no significant PL quenching was found for any metal ion (Fig. S14, ESI‡).

Time-resolved fluorescence spectroscopy was performed to reveal the influence of chemical composition on the decay kinetics (Fig. 2b). Exponential fitting of the red curve indicated that **COF2OMe** had a PL lifetime of 0.33 ns. Upon substitution of the double methoxyl side chains by cyclic 15-crown-5, 18-crown-6, and 21-crown-7, the fluorescence lifetime of the COF materials increased to 0.44, 0.53, and 0.72 ns, respectively. This increment of PL lifetime proves the suppression of the intramolecular rotational energy relaxation pathway, due to reduced conformational freedom of hydrazone bridges by the stacking of bulky and semi-rigid crown ether chains.

In conclusion, we have explored side chain engineering as a strategy to improve the PL intensity of 2D hydrazone linked COFs. By decorating the COF pore walls with cyclic crown ether chains, the PLQY of the COF material is drastically increased by 20-fold from 0.5% to 10.1%. We ascribe the PL enhancement to the eclipsed stacking crystal structure that enables the close stacking of crown ether chains. The bulky and semi-rigid characteristics of the crown ether chains result in restriction of the backbone from easy rotation or vibration around the hydrazone linkers when closely packed. The strategy here may be extended to synthesizing fluorescent COF materials with desired functions by using specific bulky or rigid side groups.

We acknowledge the NRF-CRP grant (NRF-CRP16-2015-02), funded by the National Research Foundation, Prime Minister's Office, Singapore. This work is also supported by MOE Tier 1 grant (R-143-000-B62-114) and Tier 2 grants (MOE2018-T2-1-152 and MOE-MOET2EP10120-0006).

Conflicts of interest

There are no conflicts to declare.

Notes and references

1 S. Y. Ding, M. Dong, Y. W. Wang, Y. T. Chen, H. Z. Wang, C. Y. Su and W. Wang, *J. Am. Chem. Soc.*, 2016, **138**, 3031.
2 Z. P. Li, Y. W. Zhang, H. Xia, Y. Mu and X. M. Liu, *Chem. Commun.*, 2016, **52**, 6613.
3 D. M. Li, S. Y. Zhang, J. Y. Wan, W. Q. Zhang, Y. L. Yan, X. H. Tang, S. R. Zheng, S. L. Cai and W. G. Zhang, *CrystEngComm*, 2021, **23**, 3594.
4 S. Dalapati, E. Jin, M. Addicoat, T. Heine and D. Jiang, *J. Am. Chem. Soc.*, 2016, **138**, 5797.
5 W. Zhang, L. G. Qiu, Y. P. Yuan, A. J. Xie, Y. H. Shen and J. F. Zhu, *J. Hazard. Mater.*, 2012, **221–222**, 147.
6 S. Dalapati, S. Jin, J. Gao, Y. Xu, A. Nagai and D. Jiang, *J. Am. Chem. Soc.*, 2013, **135**, 17310.
7 W. Liu, Y. P. Cao, W. Z. Wang, D. Y. Gong, T. Cao, J. Qian, K. Iqbal, W. W. Qin and H. C. Guo, *Chem. Commun.*, 2019, **55**, 167.
8 H. L. Qian, C. Dai, C. X. Yang and X. P. Yan, *ACS Appl. Mater. Interfaces*, 2017, **9**, 24999.
9 Y. Zhang, X. Shen, X. Feng, H. Xia, Y. Mu and X. Liu, *Chem. Commun.*, 2016, **52**, 11088.
10 Y. Peng, Y. Huang, Y. Zhu, B. Chen, L. Wang, Z. Lai, Z. Zhang, M. Zhao, C. Tan, N. Yang, F. Shao, Y. Han and H. Zhang, *J. Am. Chem. Soc.*, 2017, **139**, 8698.
11 M. G. Mohamed, E. C. Atayde, B. M. Matsagar, J. Na, Y. Yamauchig, K. C. W. Wu and S. W. Kuo, *J. Taiwan Inst. Chem. Eng.*, 2020, **112**, 180.
12 L. Y. Zhang, J. H. Li, H. X. Zhang, Y. Liu, Y. M. Cui, F. C. Jin, K. Wang, G. Y. Liu, Y. L. Zhao and Y. F. Zeng, *Chem. Commun.*, 2021, **57**, 5558.
13 M. G. Mohamed, M. Y. Tsai, C. F. Wang, C. F. Huang, M. Danko, L. Dai, T. Chen and S. W. Kuo, *Polymers*, 2021, **13**, 221.
14 M. G. Mohamed, N. Y. Liu, A. F. M. El-Mahdy and S. W. Kuo, *Microporous Mesoporous Mater.*, 2021, **311**, 110695.
15 M. G. Mohamed, C. C. Lee, A. F. M. El-Mahdy, J. Luder, M. H. Yu, Z. Li, Z. Zhu, C. C. Chueh and S. W. Kuo, *J. Mater. Chem. A*, 2020, **8**, 11448.
16 G. Q. Lin, H. M. Ding, D. Q. Yuan, B. S. Wang and C. Wang, *J. Am. Chem. Soc.*, 2016, **138**, 3302.
17 P. Albacete, J. I. Martínez, X. Li, A. Lo1E55ez-Moreno, S. Mena-Hernando, A. E. Platero-Prats, C. Montoro, K. P. Loh, E. M. Pérez and F. Zamora, *J. Am. Chem. Soc.*, 2018, **140**, 12922.
18 E. Q. Jin, J. Li, K. Y. Geng, Q. H. Jiang, H. Xu, Q. Xu and D. L. Jiang, *Nat. Commun.*, 2018, **9**, 4143.
19 Z. P. Li, N. Huang, K. H. Lee, Y. Feng, S. S. Tao, Q. H. Jiang, Y. Nagao, S. Irle and D. L. Jiang, *J. Am. Chem. Soc.*, 2018, **140**, 12374.
20 X. Li, Q. Gao, J. Wang, Y. Chen, Z. H. Chen, H. S. Xu, W. Tang, K. Leng, G. H. Ning, J. Wu, Q. H. Xu, S. Y. Quek, Y. Lu and K. P. Loh, *Nat. Commun.*, 2018, **9**, 2335.
21 F. J. Uribe-Romo, C. J. Doonan, H. Furukawa, K. Oisaki and O. M. Yaghi, *J. Am. Chem. Soc.*, 2011, **133**, 11478.
22 G. Zhang, Y.-l. Hong, Y. Nishiyama, S. Bai, S. Kitagawa and S. Horike, *J. Am. Chem. Soc.*, 2019, **141**, 1227.
23 K. Gottschling, L. Stegbauer, G. Savasci, N. A. Prisco, Z. J. Berkson, C. Ochsenfeld, B. F. Chmelka and B. V. Lotsch, *Chem. Mater.*, 2019, **31**, 1946.
24 Z. Kang, Y. Peng, Y. Qian, D. Yuan, M. A. Addicoat, T. Heine, Z. Hu, L. Tee, Z. Guo and D. Zhao, *Chem. Mater.*, 2016, **28**, 1277.
25 W. J. Zhang, P. P. Jiang, Y. Wang, J. Zhang, Y. X. Gao and P. B. Zhang, *RSC Adv.*, 2014, **4**, 51544.
26 G. Chen, H. H. Lan, S. L. Cai, B. Sun, X. L. Li, Z. H. He, S. R. Zheng, J. Fan, Y. Liu and W. G. Zhang, *ACS Appl. Mater. Interfaces*, 2019, **11**, 12830.
27 Y. Li, C. Wang, S. J. Ma, H. Y. Zhang, J. J. Ou, Y. M. Wei and M. L. Ye, *ACS Appl. Mater. Interfaces*, 2019, **11**, 11706.
28 L. Stegbauer, K. Schwinghammer and B. V. Lotsch, *Chem. Sci.*, 2014, **5**, 2789.
29 S. Mitra, H. S. Sasmall, T. Kundu, S. Kandambeth, K. Illath, D. D. Díaz and R. Banerjee, *J. Am. Chem. Soc.*, 2017, **139**, 4513.
30 Y. Li, C. Wang, S. Ma, H. Zhang, J. Ou, Y. Wei and M. Ye, *ACS Appl. Mater. Interfaces*, 2019, **11**, 11706.
31 W. J. Zhao, C. Y. Yu, F. Q. Chen,X. Y. Guan,H. Li, B. Tang, V. Valtchev, Y. S. Yan, S. L. Qiu and Q. R. Fang, DOI: 10.26434/chemrxiv.14157038.v1.
32 M. G. Mohamed and S. W. Kuo, *Macromolecules*, 2020, **53**, 2420.
33 X. R. Wang, X. Han, J. Zhang, X. W. Wu, Y. Liu and Y. Cui, *J. Am. Chem. Soc.*, 2016, **138**, 12332.